University of Wisconsin Milwaukee

UWM Digital Commons

May 2019

An Analysis of Momentum Flux Budgets and Profiles in a Large-Eddy Model

Steffen Domke
University of Wisconsin-Milwaukee

An Analysis of Momentum Flux Budgets and Profiles in a Large-Eddy Model

by

Steffen Domke

A Thesis Submitted in

Partial Fulfillment of the

Requirements for the Degree of

Master of Science

in Mathematics

at

The University of Wisconsin–Milwaukee

May 2019

Abstract

An Analysis of Momentum Flux Budgets and Profiles in a Large-Eddy Model

by

Steffen Domke

The University of Wisconsin–Milwaukee, 2019
Under the Supervision of Professor Vincent E. Larson

Momentum fluxes and variances play an important role in the characterization and forecast of weather phenomena, but cannot be measured easily. A subdivision of the flux changes into budget terms by the underlying physical processes, such as buoyancy transport, can assist in understanding their sources and influences. Momentum flux and variance budgets for SAM, the System for Atmospheric Modeling, have been implemented and are compared to existing budgets from other simulations.

A tool for the visualization of these quantities from three-dimensional grid data has been developed to show and explain their distribution in conjunction with shallow cumulus and stratocumulus clouds. For the shallow cumulus case, we have found opposite fluxes within clouds and in the cloud halo regions as well as a significant contribution in the environment. In a small region within the cloud layer we have upgradient fluxes.

To my family in Germany and Kristin

TABLE OF CONTENTS

LIST OF FIGURES

List of Tables

ACKNOWLEDGEMENTS

Chapter 1

Introduction

1.1 Atmospheric Simulations

Atmospheric simulations or models are complex computer programs used to calculate the state of a region of atmosphere starting from a set of boundary conditions at some point in time. As atmospheric sciences deal with a comparatively complex and chaotic subject of study, measurements and laboratory experiments can usually only focus on parts of the whole picture. Therefore, these simulations are an important tool to understand and reproduce the interconnection between different, simultaneously occurring processes in the atmosphere.

Atmospheric models are based on a set of differential equations governing the temporal and spatial evolution of the atmosphere. Restricting the calculations on a discrete grid in space and time, these equations are translated into a numerically solvable structure, which should keep the numerical error suitably small, while also minimizing computation time and hardware resources.

We distinguish between weather and climate models. Weather models simulate the atmosphere in relatively small regions of 1 to $500\,\text{km}^2$ and time intervals in the order of hours to several days, while climate simulations are used to simulate the atmosphere on a continental up to global scale and over a time of several years to decades.

Atmospheric simulations can be used for many different practical applications, ranging from the daily weather forecast to more specialized forecasts of cloud cover for solar parks or precipitation for agriculture, but also for examining large scale relationships between processes and quantities in the atmosphere, determining quantities which would be difficult to measure with conventional instruments, or verifying theoretical atmospheric models.

Subject of research for this thesis is SAM, the *System for Atmospheric Modeling*, which is used as a reference for CLUBB[1], a model that was developed by Larson et. al. CLUBB is a cloud parametrization component for climate models. It can be used as a single-column weather model for verification of the output. Therefore, both SAM and CLUBB can be used to simulate the atmosphere on a numerical grid with spatial and temporal spacing on the order of $10\,\text{m}$ and $1\,\text{s}$, respectively.

---

[1]Cloud Layers Unified By Binomials (Larson, 2017)

1.2 Momentum Flux

Momentum flux quantifies the transport of components of momentum in the atmosphere. The lifting of a horizontally moving parcel of air by buoyancy, for example, is a momentum flux. Especially for behavior of wind in combination with clouds, but also for the general prediction of mean wind, this quantity is important (see subsection 2.3.1). Its measurement, especially over a large region, is very complex, as the determination of a mean wind requires multiple or vehicle-mounted instruments. Therefore, simulating the momentum flux in an atmospheric model is a viable alternative, as it can produce data on a large number of evenly distributed grid points. Momentum flux is denoted as follows: $\overline{u_i' u_j'}$, where u refers to the wind speed, the indices $i, j \in \{1, 2, 3\}$ identify the spatial component, an overlined variable $\overline{\xi}$ indicates the mean of an instantaneous variable ξ, and a primed variable ξ' denotes the deviation from the mean, $\xi' = \xi - \overline{\xi}$. Unless stated differently, in this thesis the mean of a variable is taken over the horizontal dimension x and y, corresponding to the indices 1 and 2, respectively.

1.3 Motivation

In this thesis we will investigate momentum flux and variance budgets and profiles for the SAM model.

We will derive the second-order momentum budgets for $\overline{u'^2}$, $\overline{v'^2}$, and $\overline{w'^2}$, as well as $\overline{u'w'}$ and $\overline{v'w'}$ for SAM and compare the plots with the ones published by Heinze et al. (2015), in order to verify the output of the models.

We will see that for a particular set of boundary conditions (BOMEX), which lead to the creation of a field of cumulus clouds, the $\overline{u'w'}$ momentum flux is small within the cloud layer, while the $\overline{u'^2}$ and $\overline{w'^2}$ profiles are not. This suggests that there is some pattern in the turbulence distribution concerning cumulus clouds. We will investigate this specific structure and find an explanation for the shape of the profiles.

The calculation of the examined quantities involves averaging over the entire horizontal plane of the numerical grid. Therefore, in a horizontally inhomogeneous atmosphere a lot of information is lost. So for this thesis, a visualization program was developed, which uses the output of three-dimensional spatial grid data of SAM to create plots of the horizontal distribution of momentum, momentum fluxes, and clouds.

We will use these horizontal plots and conditional height profiles for the three regions cloud interior, cloud halo, and environment to describe the distribution of momentum and momentum fluxes associated with a field of shallow cumulus clouds. We characterize cloud halo as the volume in the immediate vicinity of the cloud interior.

Chapter 2

Basics

2.1 The System for Atmospheric Modeling

The atmospheric models discussed in this thesis is SAM, the System for Atmospheric Modeling.

Atmospheric models are complex pieces of software, which can be used to predict weather or climate, evolving from a set of boundary conditions. They can be used, among other things, for weather forecast, using the latest measurements as input and predicting the local weather development as accurately as possible, in order to plan, for example, the energy production of photovoltaic cells or wind farms. Another field of application is the verification of the current understanding of atmospheric processes. By comparing the model output with actual measurement data, researchers can investigate missing chemical or physical processes, in order to add to their knowledge of the atmospheric system.

Because of the digital nature of these models, the region and time intervals in which the atmosphere is to be simulated need to be discretized. Depending on the specific use case, the resulting grids span between 100 and more than 1×10^7 grid points, on which atmospheric variables are computed over 1×10^4 to 1×10^6 time steps, with grid point distances of 10–100,000 m and time steps of 0.1–1800 s.

SAM, the System for Atmospheric Modeling, (Khairoutdinov and Randall, 2003) was developed by Marat Khairoutdinov and is used to simulate cloud and boundary layer processes. The SAM version used at UWM is version 6.10.6. The model uses anelastic equations, meaning it includes density variations with height, instead of Boussinesq equations which approximate density to a constant, except for terms relating to gravity. The equations are implemented using the finite-difference method on a fully staggered Arakawa C-type grid. A schematic is shown in Figure 2.1. Because of the shifted subgrids, for calculations involving variables on different subgrids, these must first be interpolated onto a common grid. For time integration the model is using a third-order Adams-Bashforth method with variable time step length. For the subgrid-scale SAM uses a 1.5-order closure with an optional Smagorinsky-type scheme. In the upper third of the grid, all prognostic variables are subject to Newtonian damping, which reduces artifacts from gravity wave amplification at the rigid top grid boundary. For this thesis, it was used as a large-eddy simulation, splitting the numerical solution of the fluid dynamical differential equations into a resolved scale large-eddy part and a subgrid part,

3

approximating the influence of eddies of sizes smaller than grid distance.
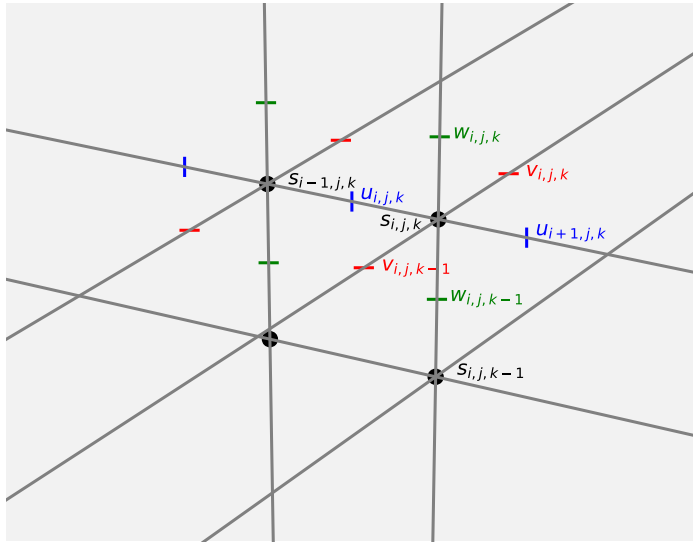
Figure 2.1: Schematic of numerical grid used in SAM. The s points denote the grid for all scalar variables. In between the scalar grid points lie the grid points of the directional momentum variables. For calculations involving variables from different subgrids, these first have to be interpolated onto a common grid. This is usually the s grid.

SAM simulates atmospheric conditions on a three-dimensional spatial grid over a large number of time steps. In a time step, the influence of the individual physical process is computed sequentially in separate subroutines. Therefore, the effect of a process on the atmospheric variables can be determined by taking the difference of the variable before and after the corresponding subroutine has been executed. We will discuss utilize this in subsection 2.3.2.

There are two different forms of SAM output data. For the profile output, the quantities are averaged over the horizontal grid points, and consequently the dimensions are time and height. This form of data is used to produce usually time-averaged height profiles.

The second form of output is a snapshot of the data at each individual grid point at a single timestep. Therefore, we have three spatial dimensions. If the simulated region of atmosphere is horizontally inhomomgeneous, information is lost by averaging, making it necessary to examine the pre-averaged data on the entire grid. In this thesis we will describe the development of a plotting tool using the snapshot data in section 3.2.

SAM output is converted to *NetCDF* files. This is a file format for storing large amounts of data, commonly used in atmospheric science. The files include metadata, such as variable names, dimension and unit information, and data description. There exist *NetCDF* interface packages for most commonly of the used programming languages.

2.1.1 Description of Cases

In order to compare different models, various sets of boundary parameters have been defined for a variety of atmospheric conditions. These are usually based on measurement campaigns, which have recorded both the boundary conditions and the subsequent development of the atmosphere.

The cases examined in this thesis are the BOMEX (Barbados Oceanographic and Meteorological Experiment) case (HOLLAND and RASMUSSON, 1973; Siebesma et al., 2003) and DYCOMS-II (Dynamics and Chemistry of Marine Stratocumulus) RF01 (Stevens et al., 2003, 2005). We will hereafter denote the cases as BOMEX and DYCOMS, respectively.

The BOMEX case consists a field of shallow cumulus clouds over the Caribbean sea. We have local regions of up- and downdraft of up to $1\,\text{m/s}$ near ground and a mean wind in eastward direction with strengths between 5 and $8\,\text{m/s}$ and a jet maximum at around $800\,\text{m}$.

THE DYCOMS case describes the boundary conditions for an almost complete cloud cover of nocturnal stratocumulus clouds at the top of the planetary boundary layer. The mean wind at ground has a strength of $7\,\text{m/s}$, increasing with height up to $9\,\text{m/s}$ above cloud top. We have bands of up- and downdrafts of up to $1\,\text{m/s}$ near ground.

2.2 Setup for Model Runs and Analyses

2.2.1 Description of UWM Supercomputers

For our simulations with the SAM model, we uses a large three-dimensional spatial grid and a simulation time interval of four to six hours. At a time step size of 1 or $0.5\,\text{s}$, we get a number of time steps in the range of 1×10^4 to 1×10^6. As a consequence, it is not feasible to run a simulation on a common desktop computer with only limited capabilities of parallelization. Hence, the model runs used in this thesis were performed on the UWM faculty research clusters *Avi* and *Mortimer*.

For a parallel run of SAM, the grid is decomposed into smaller subgrids, which are then each assigned to a processor. Usually, the horizontal plane of the grid is decomposed, so each processor is assigned a cuboid with full height levels and greatly reduced basis. Even assignments of $1 \times 1 \times n_z$ cuboids are possible, so each processor computes the simulation on one column of the numerical grid.

This reduced the computation time of the simulation runs used for this thesis ($256 \times 256 \times n_z$) to several hours instead of days. Table 2.1 shows an overview of the specifications for both the clusters used. The official description can be found at University of Wisconsin Milwaukee (2019a) and at University of Wisconsin Milwaukee (2019b).

	Avi	Mortimer
Operating System	CentOS7	CentOS7
Number of Cores	1088	1914
Number of Standard Nodes	136	83
Node Configuration	2x quad-core @2.67 GHz	2x 8/12-core @2.50 GHz
Memory	3.4 TiB	7.3 TiB

Table 2.1: Specifications for the UWM clusters on which the simulations presented in this thesis were ran.

2.2.2 Software Used for Analysis

The analysis and visualization of the model output was done with *Python* version 2.7.13 (Foundation, 2016). In order to process the data, the packages listed in Table 2.2 have been used.

Package Name	Version	Documentation	Description
netCDF4	1.3.1	Whitaker (2017)	netCDF4 is an interface for reading and writing NetCDF files
NumPy	1.16.0	community (2019)	NumPy is a library for advanced array handling and scientific computing
Matplotlib	2.2.3	Hunter et al. (2018)	Matplotlib is a library for creating plots and images

Table 2.2: List of major packages used in this thesis for data processing in *Python*

2.3 Budget Equations

2.3.1 Reynolds Averaging

When processing multi-dimensional discrete data in space and time, there are different types of averages. If not stated differently the mean will denote the average over the horizontal spatial dimensions, meaning that the data is averaged over the eastward and northward spatial axes. Usually, equations in physics are given for instantaneous quantities. This is the general form of physical laws and other forms, such as equations for mean quantities can be derived from those. In atmospheric sciences, we distinguish between mean and turbulent quantities, such as wind speed, as it is the mean quantities that define weather and climate, while turbulences usually only matter on small scales. However, we will see that the turbulent quantities influence the mean variables and so need to be included in models and simulations. The process of transforming instantaneous equations used in atmospheric sciences into equations for mean variables is called *Reynolds averaging* and will be explained using the equation for conservation of momentum, as the resulting equation will be the basis for the budgets we will discuss later on. A more in-depth description of the underlying averaging rules can be found in Stull (2012, chap. 2.4), while the summation notation used here is introduced in chapter 2.8 of the same book. The rules for this notation are, that we will implicitly summarize over each

index that occurs more than once in a term. For example, the term $x_i y_i$ is translated into $x_1 y_1 + x_2 y_2 + x_3 y_3$. The starting point is Newton's second law of motion and our goal is to derive an equation of the form $\frac{\partial \overline{u_i' u_j'}}{\partial t} = \ldots$:

$$\frac{d}{dt}(m \cdot u_i) = F_i \tag{2.1}$$

where u is the wind speed, a velocity, F the force acting on the observed system, and $i \in \{1, 2, 3\}$ the index of spatial dimensions.

Substituting the residual force with all contributing components, dividing by the mass, and applying the chain rule on the right hand side, we get:

$$\underbrace{\frac{\partial u_i}{\partial t}}_{\text{Storage}} + \underbrace{u_j \frac{\partial u_i}{\partial x_j}}_{\text{Advection}} = \underbrace{-\delta_{i3} g}_{\text{Gravity}} + \underbrace{f_c \varepsilon_{ij3} u_j}_{\text{Coriolis}} \underbrace{- \frac{1}{\rho} \frac{\partial p}{\partial x_i}}_{\text{Pressure gradient}} + \underbrace{\frac{\mu}{\rho} \frac{\partial^2 u_i}{\partial x_j^2}}_{\text{Viscous stress}} \tag{2.2}$$

where x_i ($i \in \{1, 2, 3\}$) are the spatial coordinate components, δ is the Kronecker symbol, ε is the Levi-Civita symbol, g is the gravity acceleration constant of Earth, $f_c = 2\omega \sin \Phi$ is the Coriolis parameter (ω: angular velocity of Earth, Φ: latitude), p is the pressure, and μ is the viscosity of the medium, which is air in our case. From the basis of this equation, we apply Reynolds averaging (compare Stull, 2012, chap. 3.4.3), starting with the Boussinesq approximation for shallow convection conditions (compare Stull, 2012, p. 84):

Apply Boussinesq Approximation:

$$\frac{\partial u_i}{\partial t} + u_j \frac{\partial u_i}{\partial x_j} = -\delta_{i3} \left[g - \left(\frac{\theta_v'}{\bar{\theta}_v} \right) g \right] + f_c \varepsilon_{ij3} u_j - \frac{1}{\bar{\rho}} \frac{\partial p}{\partial x_i} + \frac{\mu}{\bar{\rho}} \frac{\partial^2 u_i}{\partial x_j^2} \tag{2.3}$$

Split up instantaneous quantities:

$$\frac{\partial (\bar{u}_i + u_i')}{\partial t} + (\bar{u}_j + u_j') \frac{\partial (\bar{u}_i + u_i')}{\partial x_j} = -\delta_{i3} \left[g - \frac{\theta_v'}{\bar{\theta}_v} g \right] + f_c \varepsilon_{ij3} (\bar{u}_j + u_j') - \frac{1}{\bar{\rho}} \frac{\partial (\bar{p} + p')}{\partial x_i} + \frac{\mu}{\bar{\rho}} \frac{\partial^2 (\bar{u}_i + u_i')}{\partial x_j^2} \tag{2.4}$$

Apply Reynolds averaging rules:

$$\underbrace{\frac{\partial \bar{u}_i}{\partial t}}_{\text{Storage}} + \underbrace{\bar{u}_j \frac{\partial \bar{u}_i}{\partial x_j}}_{\text{Advection}} = \underbrace{-\delta_{i3} g}_{\text{Gravity}} + \underbrace{f_c \varepsilon_{ij3} \bar{u}_j}_{\text{Coriolis}} \underbrace{- \frac{1}{\bar{\rho}} \frac{\partial \bar{p}}{\partial x_i}}_{\text{Pressure}} + \underbrace{\frac{\mu}{\bar{\rho}} \frac{\partial^2 \bar{u}_i}{\partial x_j^2}}_{\text{Viscous stress}} - \underbrace{\frac{\partial \overline{u_i' u_j'}}{\partial x_j}}_{\text{Reynolds stress}} \tag{2.5}$$

This gives us the prognostic equation for the mean momentum in a turbulent flow. As can be seen, a new term appeared which is dependent on the components of turbulent momentum. So, in order to forecast the mean wind, we need the momentum flux, a variable dependent on turbulence.

From this we will derive a prognostic equation for the turbulent gusts. Subtracting Equation 2.5 from Equation 2.4 gives us:

$$\frac{\partial u_i'}{\partial t} + \bar{u}_j \frac{\partial u_i'}{\partial x_j} + u_j' \frac{\partial \bar{u}_i}{\partial x_j} + u_j' \frac{\partial u_i'}{\partial x_j} = \delta_{i3}\left(\frac{\theta_v'}{\bar{\theta}_v}\right)g + f_c \varepsilon_{ij3} u_j' - \frac{1}{\bar{\rho}}\frac{\partial p'}{\partial x_i} + \frac{\mu}{\bar{\rho}}\frac{\partial^2 u_i'}{\partial x_j^2} + \frac{\partial \overline{u_i' u_j'}}{\partial x_j} \qquad (2.6)$$

Multiplying Equation 2.6 by u_k' and Reynolds averaging gives us:

$$\overline{u_k'\frac{\partial u_i'}{\partial t}} + \overline{u_k'\bar{u}_j\frac{\partial u_i'}{\partial x_j}} + \overline{u_k' u_j'\frac{\partial \bar{u}_i}{\partial x_j}} + \overline{u_k' u_j'\frac{\partial u_i'}{\partial x_j}} = \delta_{i3}\overline{u_k'\left(\frac{\theta_v'}{\bar{\theta}_v}\right)}g + f_c\varepsilon_{ij3}\overline{u_k' u_j'} - \frac{\overline{u_k'}}{\bar{\rho}}\frac{\partial p'}{\partial x_i} + \frac{\mu}{\bar{\rho}}\overline{u_k'\frac{\partial^2 u_i'}{\partial x_j^2}} \qquad (2.7)$$

Adding Equation 2.7 with swapped indices i and k to itself and applying the product rule of calculus gives us the momentum flux budget equation:

$$\underbrace{\frac{\partial \overline{u_i' u_k'}}{\partial t}}_{\text{Storage}} + \underbrace{\bar{u}_j \frac{\partial \overline{u_i' u_k'}}{\partial x_j}}_{\text{Advection}} = \underbrace{-\overline{u_i' u_j'}\frac{\partial \bar{u}_k}{\partial x_j} - \overline{u_k' u_j'}\frac{\partial \bar{u}_i}{\partial x_j}}_{\text{Shear}} \quad \underbrace{-\frac{\partial \overline{u_i' u_j' u_k'}}{\partial x_j}}_{\text{Turbulent Diffusion}}$$

$$+ \underbrace{\left(\frac{g}{\bar{\theta}_v}\right)\left[\delta_{i3}\overline{u_k'\theta_v'} + \delta_{k3}\overline{u_i'\theta_v'}\right]}_{\text{Buoyancy}} + \underbrace{f_c\left[\varepsilon_{ij3}\overline{u_k' u_j'} + \varepsilon_{kj3}\overline{u_i' u_j'}\right]}_{\text{Coriolis}} \qquad (2.8)$$

$$- \frac{1}{\bar{\rho}}\left[\underbrace{\frac{\partial \overline{p' u_k'}}{\partial x_i} + \frac{\partial \overline{p' u_i'}}{\partial x_k}}_{\text{Pressure Diffusion}} \underbrace{-\overline{p'\left(\frac{\partial u_i'}{\partial x_k} + \frac{\partial u_k'}{\partial x_i}\right)}}_{\text{Return to Isotropy}}\right] + \underbrace{\frac{\mu}{\bar{\rho}}\frac{\partial^2 \overline{u_i' u_k'}}{\partial x_j^2}}_{\text{Molecular Diffusion}} \underbrace{-2\frac{\mu}{\bar{\rho}}\overline{\frac{\partial u_i'}{\partial x_j}\frac{\partial u_k'}{\partial x_j}}}_{\text{Viscous Dissipation}}$$

Based on scaling arguments we can argue, that the terms for Coriolis force, pressure diffusion, and molecular diffusion are small compared to all other terms. In the model budgets, these will usually be omitted or included in a residual term, which contains all the negligible terms and serves as a verification for the implementation of the budget.

As the indices i and k are chosen arbitrary from $\{1, 2, 3\}$, we get nine individual equations from Equation 2.8, which can be reduced to six because of symmetry (e.g. the budget equations for $\overline{u'w'}$ and $\overline{w'u'}$ are equivalent). This results in three budget equations for momentum variances: $\overline{u'^2}$, $\overline{v'^2}$, and $\overline{w'^2}$. On the other hand, we get three budget equations for the momentum fluxes: $\overline{u'v'}$, $\overline{u'w'}$, and $\overline{v'w'}$.

All six of these budgets have been implemented for SAM. In the following section, we will describe their implementation.

We can reduce Equation 2.8 even further by assuming horizontal homogeneity (Stull, 2012, chap. 3.3.4),

which gives us the following conditions for any averaged quantity $\bar{\xi}$: $\frac{\partial \bar{\xi}}{\partial x} = \frac{\partial \bar{\xi}}{\partial y} = \bar{w} = 0$.

$$
\underbrace{\frac{\partial \overline{u_i' u_k'}}{\partial t}}_{\text{Storage}} = \underbrace{-\left(\overline{u_i' w'}\frac{\partial \bar{u}_k}{\partial z} + \overline{u_k' w'}\frac{\partial \bar{u}_i}{\partial z}\right)}_{\text{Shear}} \underbrace{-\frac{\partial \overline{u_i' u_k' u_3'}}{\partial z}}_{\text{Turbulent Diffusion}}
$$

$$
+ \underbrace{\left(\frac{g}{\bar{\theta}_v}\right)\left[\delta_{i3}\overline{u_k' \theta_v'} + \delta_{k3}\overline{u_i' \theta_v'}\right]}_{\text{Buoyancy}} + \underbrace{f_c\left[\varepsilon_{ij3}\overline{u_k' u_j'} + \varepsilon_{kj3}\overline{u_i' u_j'}\right]}_{\text{Coriolis}} \quad (2.9)
$$

$$
- \frac{1}{\bar{\rho}}\left[\underbrace{\delta_{i3}\frac{\partial \overline{p' u_k'}}{\partial z} + \delta_{k3}\frac{\partial \overline{p' u_i'}}{\partial z}}_{\text{Pressure Diffusion}} \underbrace{-\overline{p'\left(\frac{\partial u_i'}{\partial x_k} + \frac{\partial u_k'}{\partial x_i}\right)}}_{\text{Return to Isotropy}}\right] + \underbrace{\frac{\mu}{\bar{\rho}}\frac{\partial^2 \overline{u_i' u_k'}}{\partial x_j^2}}_{\text{Molecular Diffusion}} \underbrace{-2\frac{\mu}{\bar{\rho}}\overline{\frac{\partial u_i'}{\partial x_j}\frac{\partial u_k'}{\partial x_j}}}_{\text{Viscous Dissipation}}
$$

2.3.2 Implementation of Budget Equations

In SAM, all influencing mechanisms (advection, Coriolis, pressure, buoyancy, dissipation) are computed sequentially in each time step. Therefore, we can calculate the change in momentum for each one by taking the difference of momentum before and after applying the respective subroutines. From this the change of momentum flux is calculated as the difference quotient restricted to the individual process *proc.*, $\frac{\Delta \overline{u_i' u_k'}}{\Delta t}\big|_{\text{proc}}$.

Budget Term	**Mechanism**	$\overline{u'^2}$ **Calculation**	$\overline{u'w'}$ **Calculation**	$\overline{w'^2}$ **Calculation**
Storage	-	$\mathcal{M} = \frac{\Delta \overline{u'^2}}{\Delta t}$	$\mathcal{M} = \frac{\Delta \overline{u'w'}}{\Delta t}$	$\mathcal{M} = \frac{\Delta \overline{w'^2}}{\Delta t}$
Turbulent Diffusion	Advection	$\mathcal{T}^t = \frac{2}{\bar{\rho}}\frac{\Delta(\bar{\rho}\cdot\overline{w' u'^2})}{\Delta z}$	$\mathcal{T}^t = \frac{1}{\bar{\rho}}\frac{\Delta(\bar{\rho}\cdot\overline{w'^2 u'})}{\Delta z}$	$\mathcal{T}^t = \frac{\Delta \overline{w'^2}}{\Delta t}\big|_{\text{adv.}}$
Shear	Advection	$\mathcal{G} = \frac{\Delta \overline{u'^2}}{\Delta t}\big|_{\text{adv.}} - \mathcal{T}^t$	$\mathcal{G} = \frac{\Delta \overline{u'w'}}{\Delta t}\big|_{\text{adv.}} - \mathcal{T}^t$	-
Buoyancy	Buoyancy	-	$\mathcal{B} = \frac{\Delta \overline{u'w'}}{\Delta t}\big|_{\text{buoy.}}$	$\mathcal{B} = \frac{\Delta \overline{w'^2}}{\Delta t}\big|_{\text{buoy.}}$
Coriolis	-	not included in SAM		
Pressure Diffusion	Pressure	-	$\Pi = \frac{1}{\bar{\rho}}\frac{\Delta(\bar{\rho}\cdot\overline{u' p'})}{\Delta z}$	$\Pi = \frac{1}{\bar{\rho}}\frac{\Delta(\bar{\rho}\cdot\overline{w' p'})}{\Delta z}$
Return to Isotropy	Pressure	$\mathcal{P} = \frac{\Delta \overline{u'^2}}{\Delta t}\big|_{\text{press.}}$	$\mathcal{P} = \frac{\Delta \overline{u'w'}}{\Delta t}\big|_{\text{press.}} - \Pi$	$\mathcal{P} = \frac{\Delta \overline{w'^2}}{\Delta t}\big|_{\text{press.}} - \Pi$
Molecular Diffusion	Diffusion	$\mathcal{D} = \frac{\Delta \overline{u'^2}}{\Delta t}\big|_{\text{diff.}}$	$\mathcal{D} = \frac{\Delta \overline{u'w'}}{\Delta t}\big|_{\text{diff.}}$	$\mathcal{D} = \frac{\Delta \overline{w'^2}}{\Delta t}\big|_{\text{diff.}}$
Viscous Dissipation	-	not included in SAM		

Table 2.3: Categorization of the individual budget terms for SAM. We subdivide the total change by advection and pressure into one part which is calculated explicitly (shear, pressure diffusion) and the other is the difference of total change less the calculated value.

Table 2.3 shows the categorization of each budget term and how it is computed. The term notation is taken from Heinze et al. (2015, p. 5). Some mechanisms encompass multiple budget terms, so for added precision, we want to distinguish, for example, between the turbulent advection and the shear term, which both are part of the total contribution by the advection mechanism. As the budget terms differ depending on w being a part of the covariance, the three different forms are listed separately with u representing both the eastward and northward horizontal component.

2.4 Cumulus Clouds

Cumulus Clouds are generally known as fair weather clouds. They form when a parcel of buoyant air at ground level rises up and is cooled in the process. When it reaches dew point temperature, the contained water vapor starts condensating, forming water droplets in the air. The latent heat released by condensation increases the temperature, and thus the buoyancy of the air. All the while cool and dry air is entrained at the upper and sideways boundary of the air parcel, causing a mixing and cooling in the boundary region. As a consequence of pressure compensation, we get a region of downdraft enclosing the rising air
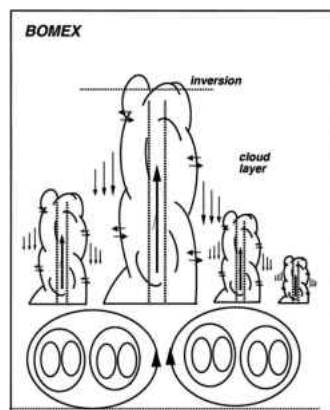

Figure 2.2: Schematic of the momentum distribution for BOMEX. Image taken from Siebesma et al. (2003). The cloud cores contain strong updraft, while there is downdraft in the surrounding region, the halo. We have entrainment at the boundaries and a turbulent subcloud layer. Additionally, while cloud base is at roughly equal height for each cloud, but cloud tops are spread over a larger region.

parcel and forming a barrier between the buoyant air and the environment. Figure 2.2 shows a schematic taken from Siebesma et al. (2003) describing the makeup of the atmosphere in the simulated region.

A question that arose from the output statistics of the simulations was how a field of cumulus clouds would interact with the environment. Would a cloud form a movable obstacle for the ambient wind and force it to flow around the boundaries, all the while drifting in the direction of the mean wind or would the cloud exhibit an inertial resistance to the wind, and in so doing, lag behind the mean wind? Or would the cloud be permeable to the mean wind and not interact with it, and consequently retain the original characteristics of the buoyant air parcel near ground level? We will investigate these questions by analyzing the height profiles and the three-dimensional data produced by SAM in section 4.2.

Chapter 3

Discussion of Budgets and Plots

3.1 Simulation Runs

The simulation runs for this thesis were done on the UWM cluster *mortimer*. In section 4.1 the results provided by SAM will be compared to those published in Heinze et al. (2015). The simulation parameters for both the SAM simulations and those performed by Heinze et al. are listed in Table 3.1. The setup for the SAM runs is taken from Siebesma et al. (2003) for BOMEX and Stevens et al. (2005) for DYCOMS with the exception that the number of horizontal grid points was increased to 256×256, in order to smooth horizontal means. Note that the runs used in this thesis have a smaller and coarser spatial grid compared to the runs presented by Heinze et al., who use a 1280×1280 horizontal grid with spacing of $5\,\mathrm{m}$ in all three directions, with 640 and 320 for BOMEX and DYCOMS, respectively.

	SAM		Heinze et al.	
	BOMEX	**DYCOMS-II RF01**	**BOMEX**	**DYCOMS-II RF01**
Time Steps	21,600	28,800	-	-
Time Step Size	$1\,\mathrm{s}$	$0.5\,\mathrm{s}$	-	-
Horizontal Grid Points	256×256	256×256	1280×1280	1280×1280
Horizontal Grid Spacing	$100\,\mathrm{m}$	$35\,\mathrm{m}$	$5\,\mathrm{m}$	$5\,\mathrm{m}$
Vertical Grid Points	75	320	640	320
Vertical Grid Spacing	$40\,\mathrm{m}$	$40\,\mathrm{m}$	$5\,\mathrm{m}$	$5\,\mathrm{m}$
Sampling Interval	181–$360\,\mathrm{min}$	61–$180\,\mathrm{min}$	181–$360\,\mathrm{min}$	121–$240\,\mathrm{min}$
Sample Size	180	120	540	360
3D Data Sampling	360–$360\,\mathrm{min}$	240–$240\,\mathrm{min}$	-	-

Table 3.1: Comparison of simulation parmeters used for SAM runs and by Heinze et al.

3.2 Description of Plotting Software

In order to get information from the raw data output by SAM, the Larson group has developed a plotting software which, in its last iteration has been implemented in *Python*. This software uses the two-dimensional output to plot height profiles of the simulated quantities, which are used describe and visualize the overall status of the volume of atmosphere. However, especially for boundary conditions resulting in a horizontally inhomogeneous atmosphere, such as the BOMEX case, averaging over the entire horizontal plane will elim-

inate information about that inhomogeneity. To analyze the distribution of momentum fluxes associated with cumulus clouds, a plotting software for the three-dimensional snapshot output has been developed.

The resulting plots should visualize the differences in wind direction, turbulence, and momentum flux within clouds, in their halo region, and in the environment. The plots should show these quantities in all three spatial dimensions; however, as we want to specifically view the horizontal differences, the plots will show slices in the x-y plane of the simulation grid. In the future, we could also implement an option to show the atmospheric development in time. The option to output three-dimensional data at various time steps already exists in SAM.

3.2.1   Algorithm

In this section, we will describe the algorithm of the program.

We start by reading the data necessary for the plots from the given *NetCDF* files. This includes the numerical data itself, but also descriptions and units. The data which is read from the output files is listed in Table 3.2.

3D data		2D data	
u	Eastward wind component	$\overline{u'w'}$	Eastward momentum flux
v	Northward wind component	$\overline{v'w'}$	Northward momentum flux
w	Vertical wind component		
q_n	Liquid water content		

Table 3.2: Data needed from *NetCDF* files: The **2D data** entries are read from the profile output of SAM, and are already interpolated and horizontally averaged. **3D data** entries are read from the three-dimensional output of SAM. They are neither interpolated nor averaged.

As a next step, the data is processed to be plotted. SAM uses different grid placements for the wind and the scalar variables, also shown in section 2.1. As the profile data is interpolated to the scalar grid, while the three-dimensional data is not, we need to interpolate the latter for our calculations.

We calculate from the three-dimensional output the mean wind components, the scalar values for horizontal mean wind strength and direction, local turbulences and momentum fluxes, and finally conditional masks for clouds, halo and environment based on the liquid water content q_n. We define the cloud region as all grid points, whose value for q_n is greater than a limit value. In our case, we use 0 as limit. The result is a three-dimensional boolean array, which is later used to plot contours of the cloud region and index the data arrays for conditional averaging.

Defining the halo region is done by binary dilation[1] of the cloud mask with a square symmetric bipyramid structuring element with corners on the axes. Figure 3.1 shows the structuring element for a dilation length

---

[1](Wikipedia contributors, 2019)

of 2, which is at the same time the result of a dilation applied to a binary array[2] with a single 1 at the point (i,j,k). The dilation grows the regions comprised of 1s according to the structuring element. Unfortunately, this is a rather inaccurate way of establishing the halo region, as we will see in the plots. A better method would be to infer the halo region from model data. In theory, using the vertical wind component would be a viable alternative. However, as we will see in the plots, a negative vertical wind component is not only found in the vicinity of clouds. The dilated mask determines the combined regions of cloud and halo. Subtracting the cloud mask gives us the halo mask. While taking the boolean complement of the combined mask gives us the environment mask.
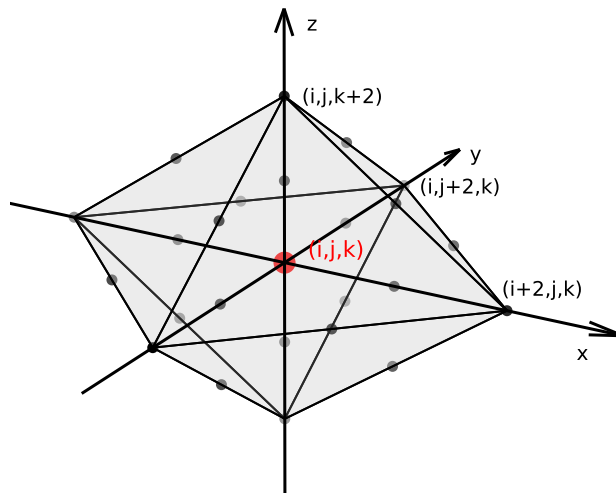

Figure 3.1: Structuring element for a dilation length of 2. This volume element is used to grow regions in a binary array. Dilating a single 1 at point (i,j,k) will result in exactly this structuring element.

Following this, we prepare the objects needed for plotting, such as colormaps and handlers, which will control the generation of the images for each height level, combining them to an animation file as well as a `pdf` file containing the individual plots. A segmented colormap is set up for the background image, based on the data to be plotted. The momentum flux data contain outliers, which need to be excluded from the color mapping, in order to improve readability of the plots. We project negative values onto a red color, positive values onto green, values close to 0 onto white.

For each height level, we call a function `update_plot`, which handles the data processing for the corresponding horizontal grid slice and generates the plot. The conditional averages are computed by indexing with the three masks and averaging, and finally, the plot content is generated:

- The background map and its associated colorbar displays either the vertical wind component or the

---

[2]An array containing only the values 0 and 1. In most programming language this is equivalent to boolean array. In `NumPy` such a mask can be used as index field for arrays.

local momentum flux $u'w'$ or $v'w'$

- Arrows representing the strength and direction of the horizontal total wind or deviation from the mean horizontal wind

- The profile plot containing the cloud fraction information as background color and the layer averaged $\overline{u'w'}$ and $\overline{v'w'}$ momentum flux profiles.

After handling each individual height level, the profiles for the conditional averages for momentum and momentum fluxes in the three regions cloud interior, halo, and environment are generated. And output with the profile plotting tool mentioned above.

In the following two sections, we will describe the output of the program explained above. subsection 3.2.2 will cover the visualization of the horizontal data slices, while subsection 3.2.3 will cover the conditional profiles created from the three-dimensional data.

3.2.2 Description of Horizontal Plots

Figure 3.2 shows an example output of the program described in section 3.2 for the BOMEX case. The plot on the right shows a height profile for the simulated atmospheric region. The arrow indicates the height of the depicted horizontal slice. Using the colormap `Blues` from the package `Matplotlib`, the background color indicates the fraction of cloud cover at each height level, ranging from white to blue, representing $0\,\%$ and the maximum cloud fraction found in the data, respectively. The lines shown in that plot are the layer averaged $overline u'w'$ (green) and $\overline{v'w'}$ (red) momentum flux profiles taken from the profile output of SAM.

The plot on the left shows data for the horizontal slice at the height level indicated by the arrow in the right-hand plot and noted in the title. The arrows shown at each grid point in the left-hand plot in Figure 3.2 represent the total horizontal wind at the indicated grid point, while the arrows in Figure 3.3 represent the horizontal turbulence, or deviation from the horizontal mean.

In the region around grid point $(10\,\mathrm{km}; 10\,\mathrm{km})$, we can see two contour lines. The blue, inner contour line encloses the hatched cloud region. The grey, outer contour delimits the halo region of clouds. The size of the halo region in this plot is 4 grid points, which corresponds to $400\,\mathrm{m}$ in the horizontal and $160\,\mathrm{m}$ in the vertical direction. In Figure 3.2 and Figure 3.3, the background color represents the vertical wind speed. The colorbar on the right-hand border shows the mapping used. For example, at grid point $(11\,\mathrm{km}; 25\,\mathrm{km})$, we have a large updraft of around $3\,\mathrm{m/s}$, while at grid point $(11\,\mathrm{km}; 17.5\,\mathrm{km})$ we have a large downdraft of around $-1.5\,\mathrm{m/s}$.

Figure 3.4 and Figure 3.5 show horizontal slices for DYCOMS data. Figure 3.4 depicts the atmosphere just below cloud cover. Similar to the cumulus clouds of BOMEX, the stratocumulus are mostly localized

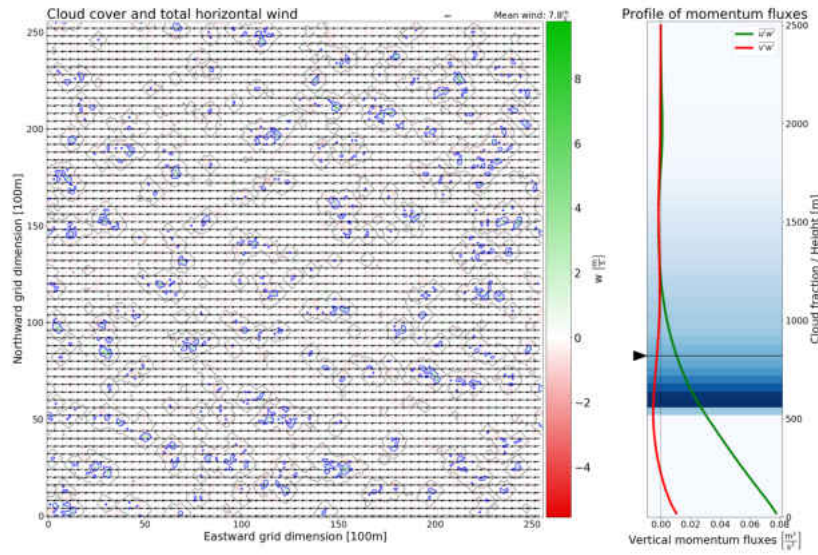total horizontal wind+w map, BOMEX, 256x256x63, dx=100m, dz=40.0m, t=360min, h=820.0m

Figure 3.2: Example frame for horizontal plots for BOMEX at height $820\,\mathrm{m}$. The plot on the right shows the profiles for momentum fluxes, the cloud fraction by background color, and the height of the examined horizontal slice by the arrow indicator. The plot on the left contains contours for the cloud and halo regions, arrows as horizontal wind indicator, and background color for the vertical wind component, as described by the colorbar.

in the updraft regions. We have strong horizontal perturbations with no favored direction. Figure 3.5 shows the clouds covering up- and downdraft regions and even stronger perturbations arranged in fields pointing in the same direction. Regions without cloud cover have little vertical momentum.

horizontal wind perturbation+w map, BOMEX, 256x256x63, dx=100m, dz=40.0m, t=360min, h=820.0m
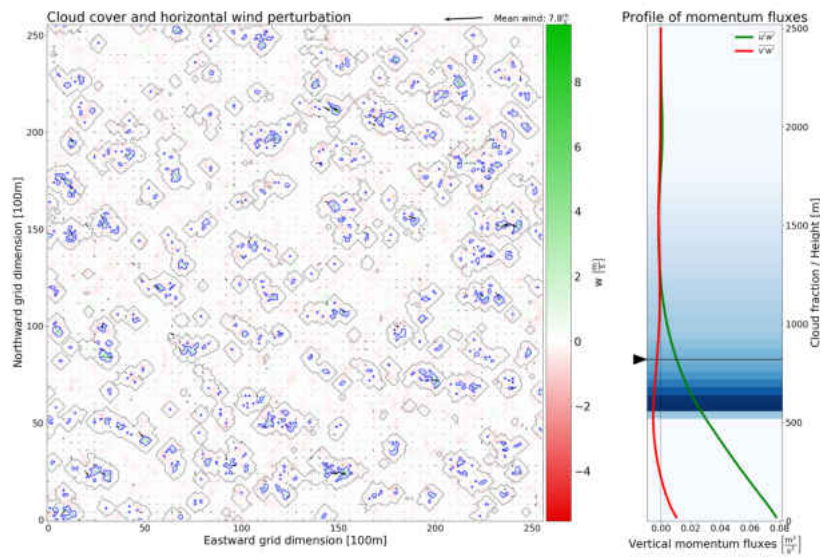
Figure 3.3: Example frame for horizontal plots. The layout and data shown are the same as Figure 3.2, with the exception, that the arrows in the left plot represent the horizontal wind perturbation. In the vicinity of clouds, for example at around (15 km, 21 km), we see large horizontal turbulence, mostly directed against the mean wind. The local wind is weaker than the mean wind.
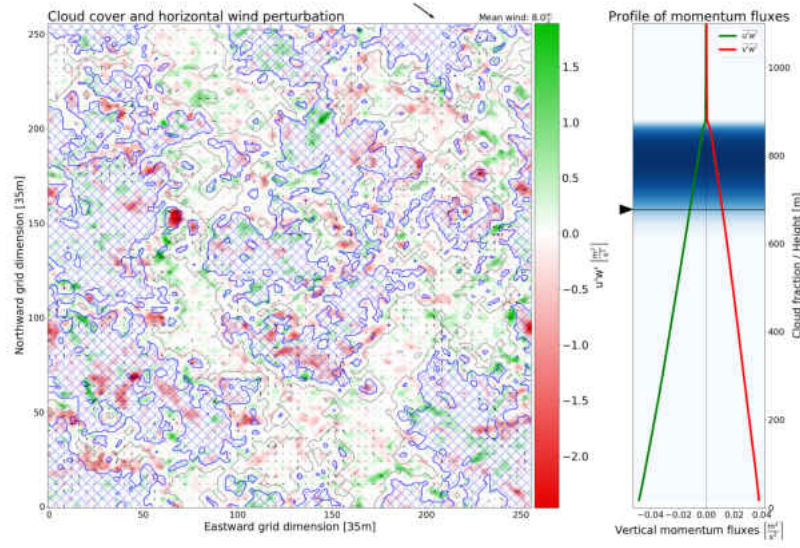
Figure 3.4: Example frame for horizontal plots. Shown is a slice of DYCOMS data just below cloud cover at height 677.5 m. Similarly to the cumulus clouds in BOMEX, the lower parts of these stratocumulus clouds are located in updraft regions. Throughout the plane, we see strong horizontal perturbations with no favored direction.
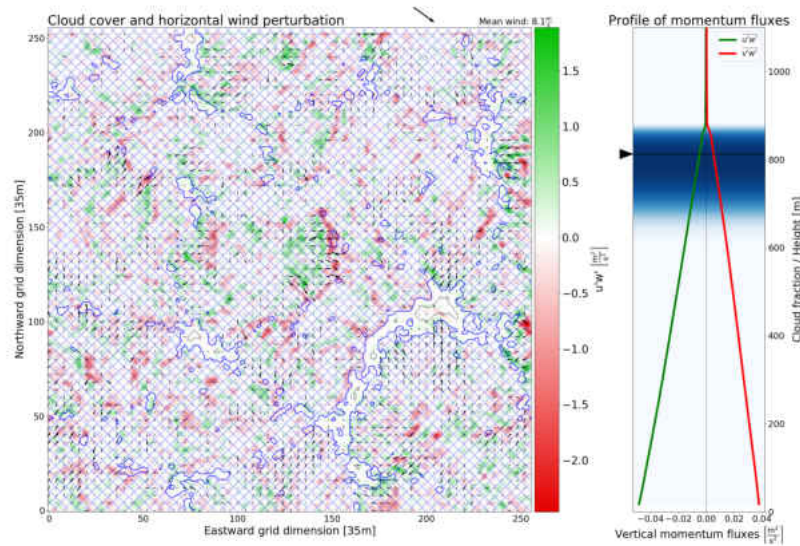

Figure 3.5: Example frame for horizontal plots. Shown is a slice of DYCOMS data within cloud cover at height 812.5 m. The clouds encompass both up- and downdraft regions now, while regions with little vertical momentum are cloud free. We now have even stronger, more localized horizontal perturbations.

3.2.3 Description of Conditional Profile Plots

The plots shown in this section were also produced by the tool described in subsection 3.2.1. As mentioned above, the values at the individual grid points are averaged conditionally based on the presence of water vapor at or in the vicinity of each point, which correspond to cloud and halo conditions, respectively. The red, green, and blue dashed lines represent the conditional means within cloud, within the halo, and in the environment, respectively. The black solid lines are the sum of all three conditional means, and therefore the unconditional mean. Figure 3.6 shows the conditional profiles generated from the snapshot data for $\overline{u'w'}$ on the left and $\bar{u}$ on the right. Most of the $\overline{u'w'}$ flux is contained in clouds. We see a lag in wind speed within clouds with height which we will use to show upgradient flux within clouds in subsection 4.2.1. The plots will be described in more detail in section 4.2.
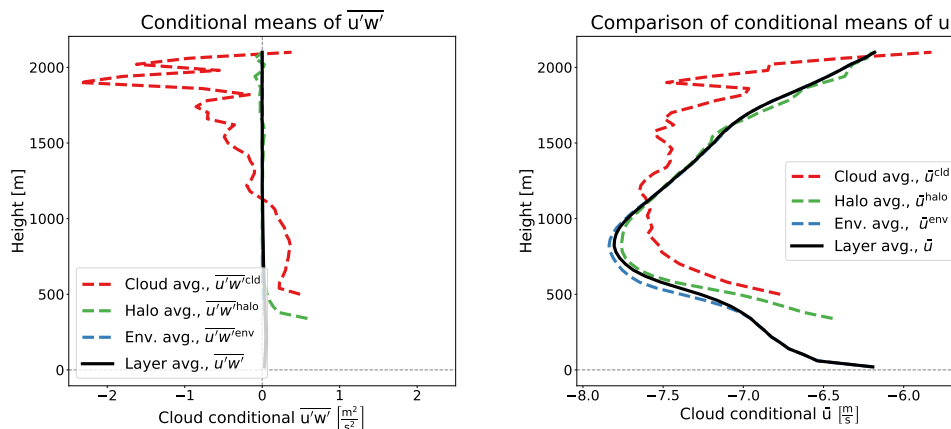

Figure 3.6: Cloud-conditional profiles for BOMEX case. The left-hand plot shows conditional $\overline{u'w'}$ momentum flux. We see, that the in-cloud flux is much larger than in the environment. Since the cloud cover is only around 5 %, the in-cloud flux does not influence the total flux significantly. The right-hand plot shows the conditional mean wind. We see a lag in z-direction of the in-cloud mean with a local maximum at around 1200 m.

Chapter 4

Momentum Analysis

4.1 Comparison of Second-Moment Budgets

Figure 4.1 and Figure 4.3 show the $\overline{u'w'}$ and $\overline{v'w'}$ budgets based on the profile output from SAM and Figure 4.2 those provided by Heinze et al. (2015). The linestyles for both the SAM and Heinze budget plots match for the common terms. The time tendency term, which is unique to SAM budgets here, has been given a grey color and is small in all the plots shown, as was predicted by Heinze.

4.1.1 Momentum Flux Budgets

In budgets from Heinze et al., we see, that near the ground the budget terms diverge strongly, while the SAM buoyancy and turbulent production terms generally have an extremum and the pressure terms have the opposite sign. This might indicate, that splatting is handled differently for both models. Splatting refers to the redirection of momentum at a barrier. For example, if a downdraft hits the ground, the momentum is not lost, but instead is converted to horizontal momentum. So at the ground we would expect a high amount of momentum flux where we have vertical momentum. We can see the more prominent spikes at cloud top for DYCOMS, as we have an almost complete cloud cover and a fairly well defined cloud layer. In contrast, for BOMEX, the atmosphere contains a large number of separated cumulus clouds, the height of which depends on the local conditions. It follows, that not all cloud tops will be at the same height, but are distributed throughout a larger vertical region. Consequently, we have a less clear progression of the profile above cloud base, starting at approximately 500 m. We will see this behavior again in subsection 4.2.3, where we can see several cloud tops at the height shown, but others reaching far higher. For the BOMEX case, we observe that the values in Heinze's plots above cloud base are larger by a factor of about 2. Especially noticeable is the difference between the peaks of the turbulent production term in the $\overline{v'w'}$ budget. The peaks at 300 m have similar size, while the ones at 600 m differ by a factor of 2. For DYCOMS, no such scaling factor is found. This factor might be a consequence of the different grid configurations used. Because of the inhomogeneous atmospheric makeup for BOMEX, the smaller grid spacing should yield more accurate results.

For BOMEX, the terms present in both the Heinze and SAM budget profiles shown in Figure 4.2 (a and c) and Figure 4.1 have a generally good agreement. We have a similarly good agreement for the DYCOMS profiles shown in Figure 4.2 (b and d) and Figure 4.3. As described by Heinze, the dissipation and time tendency terms are small and have been included in the residual for their budget. For both cases the residual terms differ, especially near ground level. The Heinze residual is significant near ground, while for all profiles shown the SAM residual is negligible. Comparing $\overline{v'w'}$, we have large fluctuations in Heinze's budget starting at around 1000 m, which are not present in the SAM budget, but on average the terms show similar tendencies.
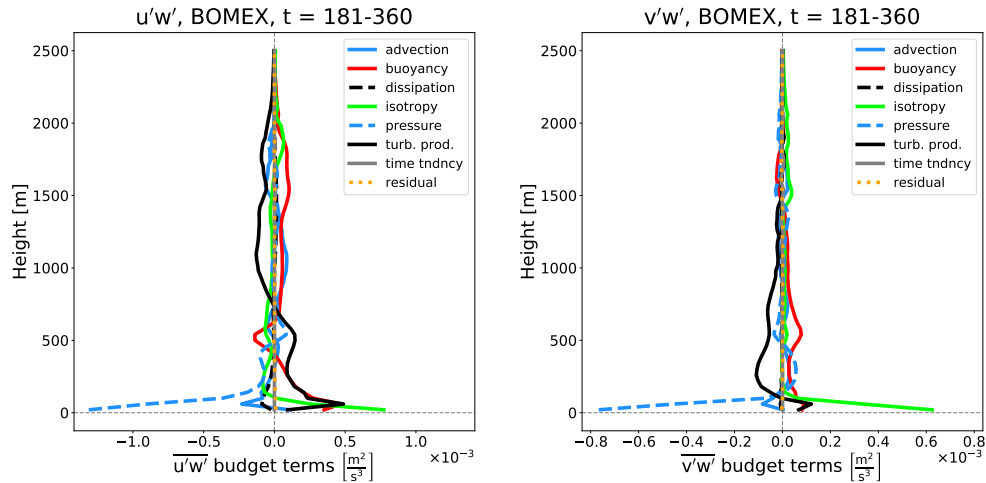

Figure 4.1: Momentum flux budget plots for BOMEX case from SAM output: Comparing to Figure 4.2, we have rough agreement for all terms, except near ground level, where the $\overline{u'w'}$ buoyancy and turbulent production terms for BOMEX change direction near ground and the pressure term has the opposite sign. The Heinze terms are scaled by a factor of 2 above cloud base. The large fluctuations above 1000 m present in the Heinze $\overline{v'w'}$ terms is absent in the SAM terms.
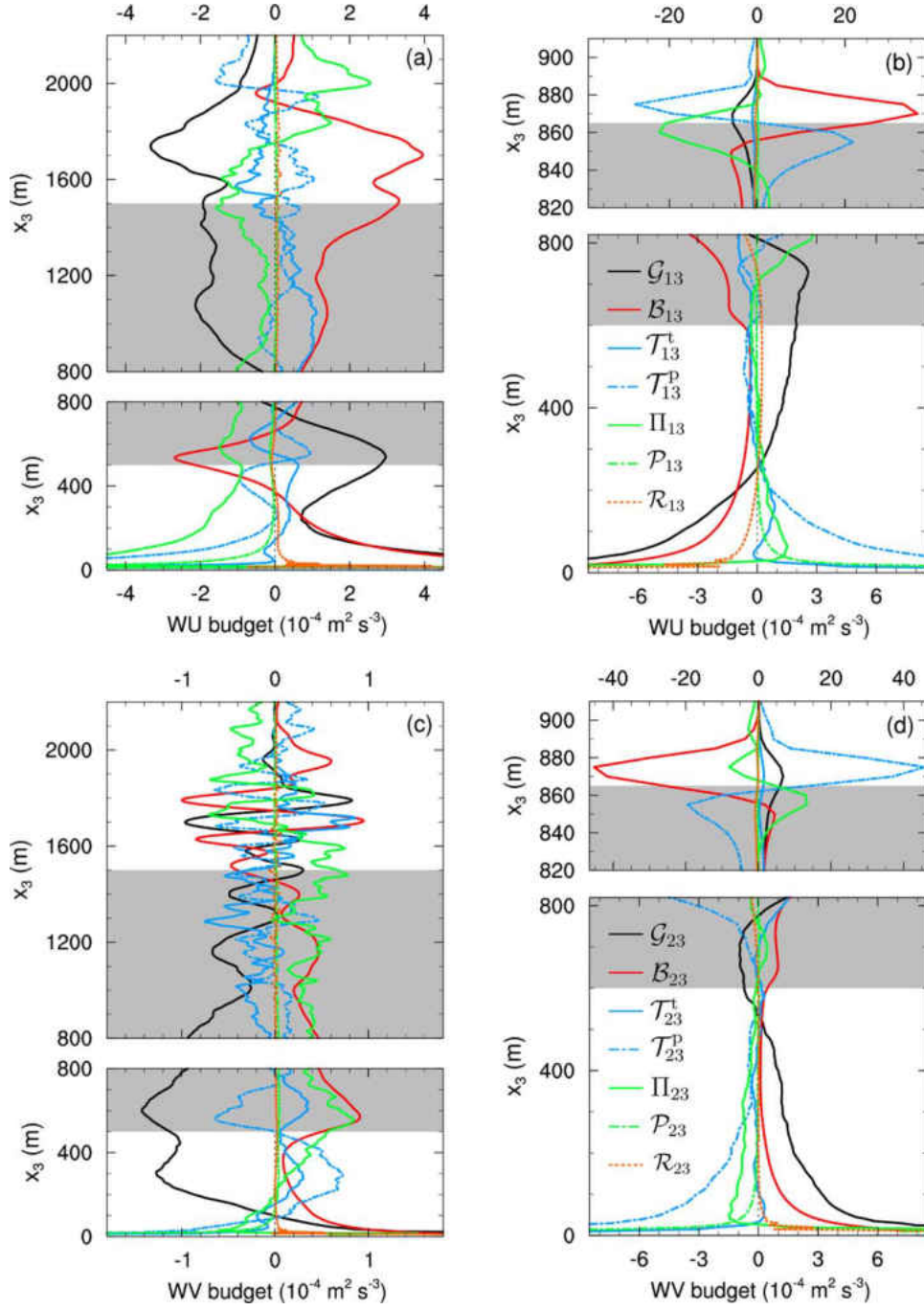
Figure 4.2: Momentum flux budget plots case taken from Heinze et al. (2015). BOMEX budgets are shown in subplots (a) and (c), DYCOMS budgets are shown in subplots (b) and (d). According to Heinze et al., the disspiation, Coriolis, and time tendency terms are negligible and therefore not plotted.
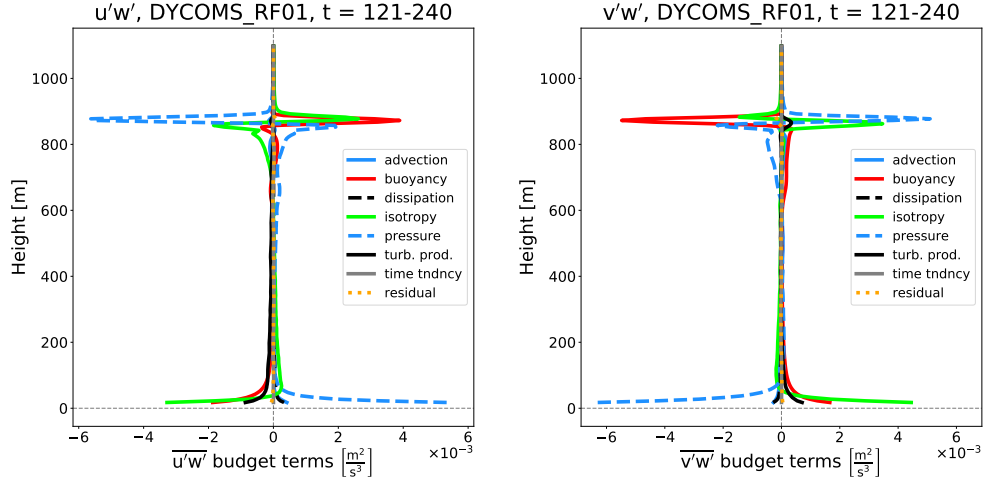
Figure 4.3: Momentum flux budget plots for DYCOMS case from SAM output: Comparing to Figure 4.2, we have good agreement in all terms for both $\overline{u'w'}$ and $\overline{v'w'}$ budgets.

4.1.2 Momentum Variance Budgets

For comparison of the variance budgets shown in Figure 4.4, Figure 4.5, and Figure 4.6, the $\overline{v'^2}$ budget was omitted, as the individual terms are very similar to the corresponding terms in the $\overline{u'^2}$ budget.

Again, we can see a good agreement in the common terms, except near ground for BOMEX, where some terms have extrema, such as turbulent production in $\overline{u'^2}$ and others are small, such as pressure in $\overline{u'^2}$. The $\mathcal{P}$ (dotted) term in the Heinze plots can not be matched, as it is the subgrid contribution to the pressure redistribution term Π (solid) and we do not output subgrid terms for SAM. For BOMEX, there is no scaling factor between the SAM and Heinze terms in the variance budgets.
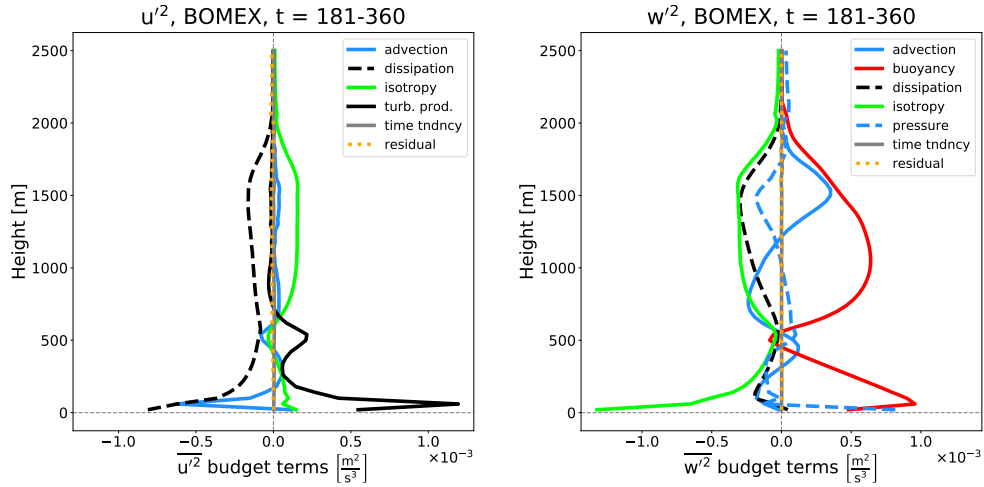
Figure 4.4: Momentum variance budget plots for BOMEX from SAM profile output: The $\overline{v'^2}$ budget has roughly the same form as the $\overline{u'^2}$ budget. Both the $\overline{u'^2}$ and $\overline{v'^2}$ budget terms show very differing behavior near ground. All Heinze terms diverge in a similar manner, while the SAM terms have an extremum, are small, or even have opposite signs.
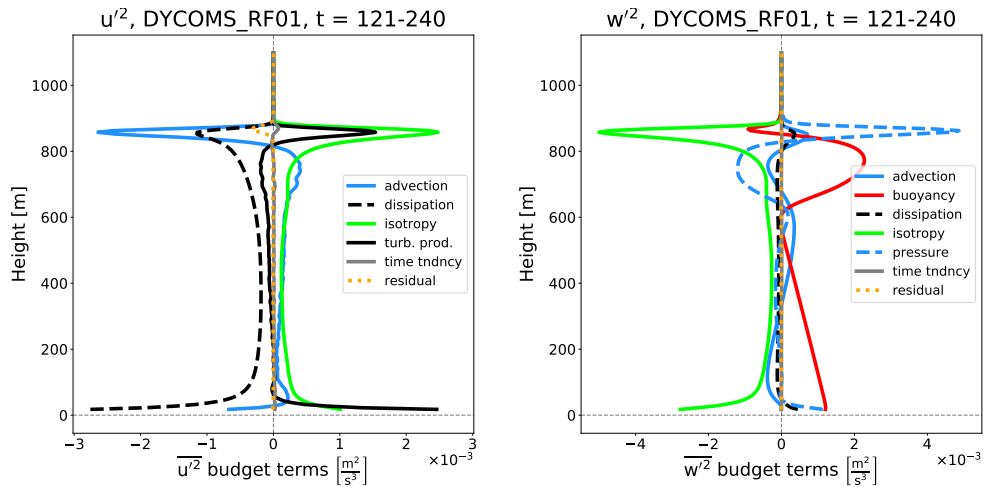

Figure 4.5: Momentum variance budget plots for DYCOMS from SAM profile output: The $\overline{v'^2}$ budget has roughly the same form as as the $\overline{u'^2}$ budget.
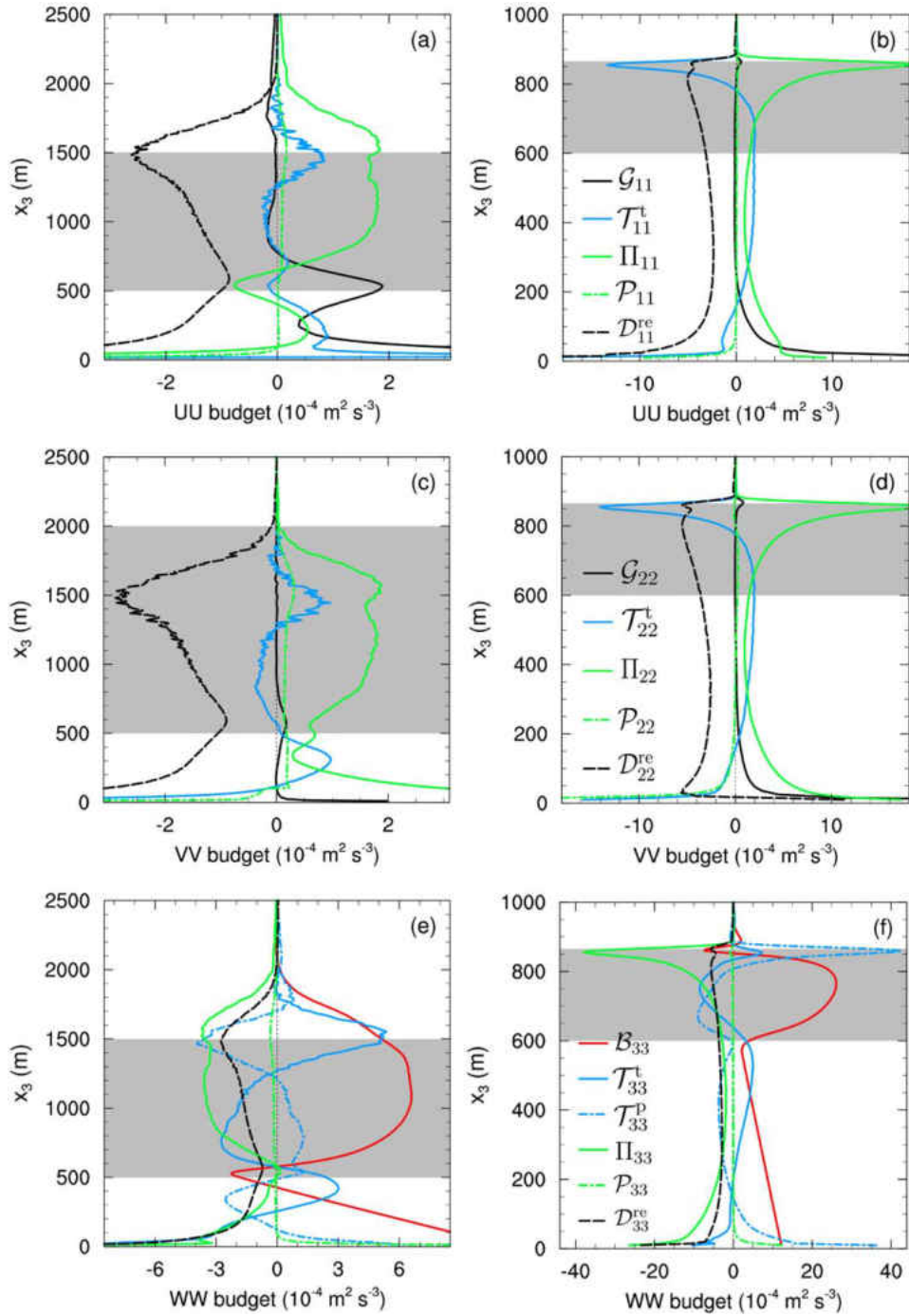
Figure 4.6: Momentum variance budget plots taken from Heinze et al. (2015). BOMEX budgets are shown in subplots (a), (c), and (e), DYCOMS budgets are shown in subplots (b), (d), and (f). Coriolis and time tendency terms are negligible and therefore not plotted. The dissipation terms $\mathcal{D}^{re}$ are calculated as the residuals of the other terms shown.

4.2 Horizontal Momentum Distribution

In this section, we will analyze the distribution of momentum fluxes for the BOMEX case. Inherent to the BOMEX case, we have a jet in the mean eastward wind profile with a minimum at about $800\,\text{meter}$ and localized buoyant air, which leads to the creation of cumulus clouds. Due to this specific conditions, we have found an upgradient flow. In general, fluxes are said to be downgradient, as there is always a force working towards homogeneous distribution of the examined quantity. As we have seen in subsection 2.3.1, momentum fluxes do influence the mean quantities, so atmospheric simulations need to account for these fluxes. A possible approximation used in simulations is based on the assumption, that fluxes are downgradient. This approach is called *Gradient Transport Theory* and is described in Stull (2012, chap. 6.4.1). Hence, the flux of a quantity ξ is approximated by the following equation:

$$\overline{u_i'\xi'} = -K\frac{\partial\bar{\xi}}{\partial x_i} \tag{4.1}$$

where $K > 0$ is some constant to be determined. However, the pronounced jet structure of the wind profile of BOMEX combined with the inertia of the rising air parcel leads to a region above the jet maximum having upgradient momentum fluxes, showing that for specific conditions, the assumption of downgradient fluxes does not hold (see Figure 4.7).

4.2.1 Conditional Wind Profiles

Comparing the conditional average of the eastward wind with the total mean in the left-hand panel of Figure 4.7, we see a lag with height of the in-cloud mean, caused by inertia. The transfer of momentum from the surrounding air to the rising air parcel is not instantaneous. We can conclude, that clouds are not permeable for wind, but momentum is being transferred while the air parcel continues rising. It forms a movable obstacle.

In the right-hand plot, we see a magnified section around the jet maximum. At height $750\,\text{m}$, u' and w' are both positive, while the gradient $\frac{d\bar{u}}{dz}$ is negative. Hence, the flux is downgradient here. However, at height $900\,\text{m}$, above the jet maximum, the gradient $\frac{d\bar{u}}{dz}$ is negative, although u' and w' are still positive. We get an upgradient flux.

We see a huge variation in the cloud-conditional profiles above $2100\,\text{m}$. This is due to the low cloud fraction at these heights. The data used in these profiles is not time-averaged, as the snapshot data is only taken from a single time step. Sampling three-dimensional data over a longer time interval of around an hour should reduce the noise and clear up the profiles in this height region.
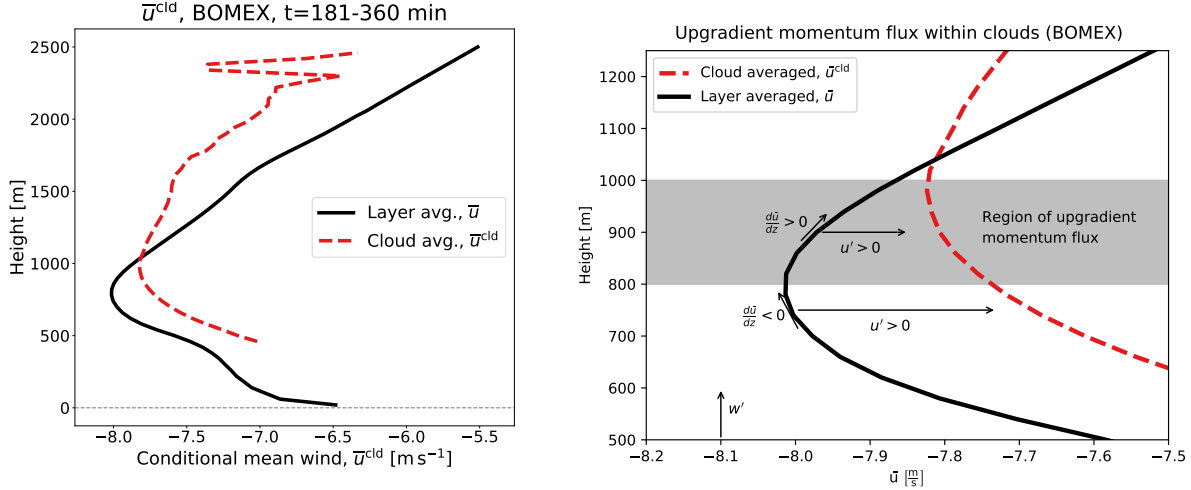
Figure 4.7: Comparison plots for horizontal mean wind profiles. For both eastward and northward wind directions we observe a lag of the in-cloud mean wind behind the total mean wind. This leads to the conclusion, that clouds form a barrier to the environmental wind and exert some resistance against the environmental wind. The transfer of momentum is not instantaneous. This leads to a region within clouds, where we get flux, that is directed up-gradient.

The question is then, if there is any connection between momentum variances and fluxes. We will discuss this in the following section.

4.2.2 Second-Moment Profiles

Comparing the BOMEX second-moment profiles in Figure 4.8, which show the SAM profile output, we see that the $\overline{u'w'}$ momentum flux is very small at around 1000 m and above, and changes signs in the 1200 to 1700 m range. This lower boundary coincides with the intersection between conditional and total mean eastward wind, as shown in Figure 4.7. At the same time, $\overline{u'^2}$ and $\overline{w'^2}$ are still very large up to a height of around 2000 m. This suggests that there is some structure in the wind field, which causes contributions from the individual grid points to the momentum flux to cancel out. Since total means will eliminate information about the distribution of momentum flux, we will analyze the plots of horizontal slice and conditional profile plots created by the tool described in section 3.2. The resulting plots are shown and discussed below.

4.2.3 Plots of Horizontal Grid Slices

The plots shown in this section will highlight the distribution of momentum and momentum flux in the atmosphere when cumulus clouds are present. We will first establish, the distribution of vertical momentum around clouds. Figure 4.9 shows the slice of the simulated atmosphere at height 1020 m. The background
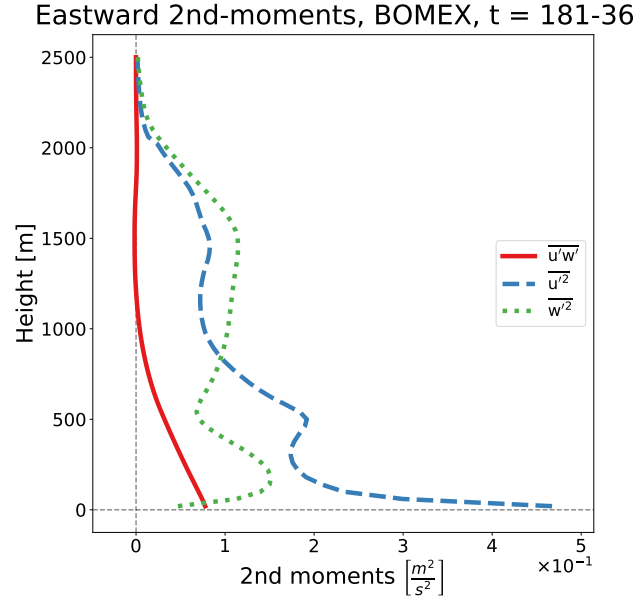
Figure 4.8: Comparison of second-moment profiles for BOMEX case from SAM profile output. We see the blue and green variance profiles, $\overline{u'^2}$ and $\overline{w'^2}$ are significant between $1000\,\mathrm{m}$ and $2000\,\mathrm{m}$, while the flux profile is small at the same heights.

color represents the vertical wind component. The interior of clouds contains strong updrafts, and fairly chaotic regions of downdrafts in the vicinity. However, between and above clouds the vertical wind is not zero. In these regions we would expect no vertical momentum, as the influence of the ground is negligible and the buoyant air is contained in the cloud regions. These deviations might be due to clouds causing gravity waves.

Figure 4.10 shows the atmospheric slice at height $1020\,\mathrm{m}$, which is the same height as in Figure 4.9. The background colors represent the local eastward momentum flux. We see, that for most clouds, we have large positive contributions, but for some smaller cloud regions, which are near their cloud tops, we have negative contributions. The vertical momentum is still upwards, but the arrows show, that the eastward turbulence is negativ now. This implies that in these regions the local eastward wind is stronger than the total horizontal mean. This can be explained by the wind of the environment being forced to flow around the cloud obstacle, so it must increase in velocity. This effect is superimposed by a strong divergence at cloud top due to the upward momentum terminating and air being pushed to the sides. Additionally, there is a highly asymmetric halo region around clouds with negative contributions. Different clouds seem to have a region of interaction, where we have smaller significant values of flux, which would suggest that momentum flux outside of the extended cloud region is not necessarily negligible. In summary, the largest contributions to the momentum flux are found in or around clouds. The contributions of different clouds, or even different regions of one

horizontal wind perturbation+w map, BOMEX, 256x256x63, dx=100m, dz=40.0m, t=360min, h=1020.0m
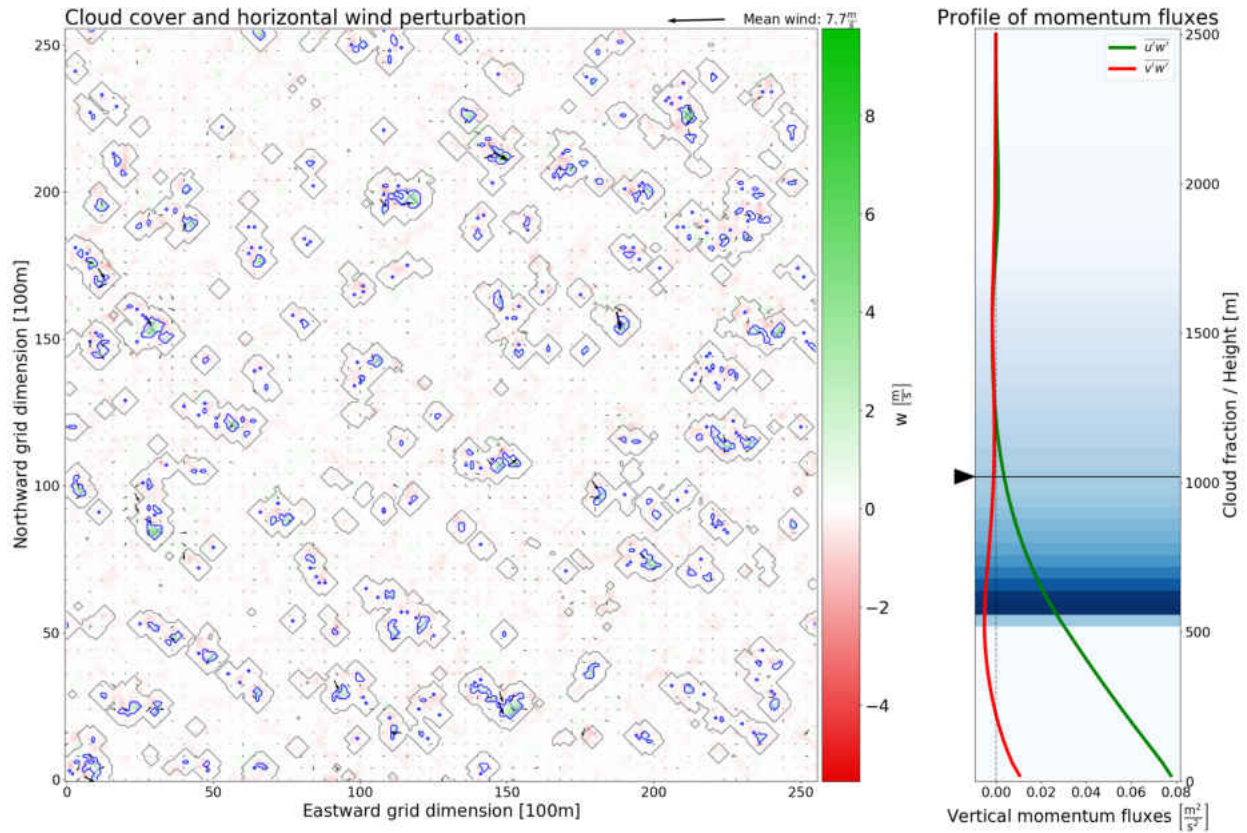

Figure 4.9: Horizontal slice, BOMEX, h = 1020 m, w background. At this altitude, we see midsections and tops of clouds. The strong updrafts are located inside clouds, while we have strong downdrafts in the northern part of the halo regions. The halo regions in this image is the 4 grid point neighborhood of clouds, which corresponds to 400 m.

cloud, cancel out. This leads to the total momentum flux being very small, even though the variances are large.

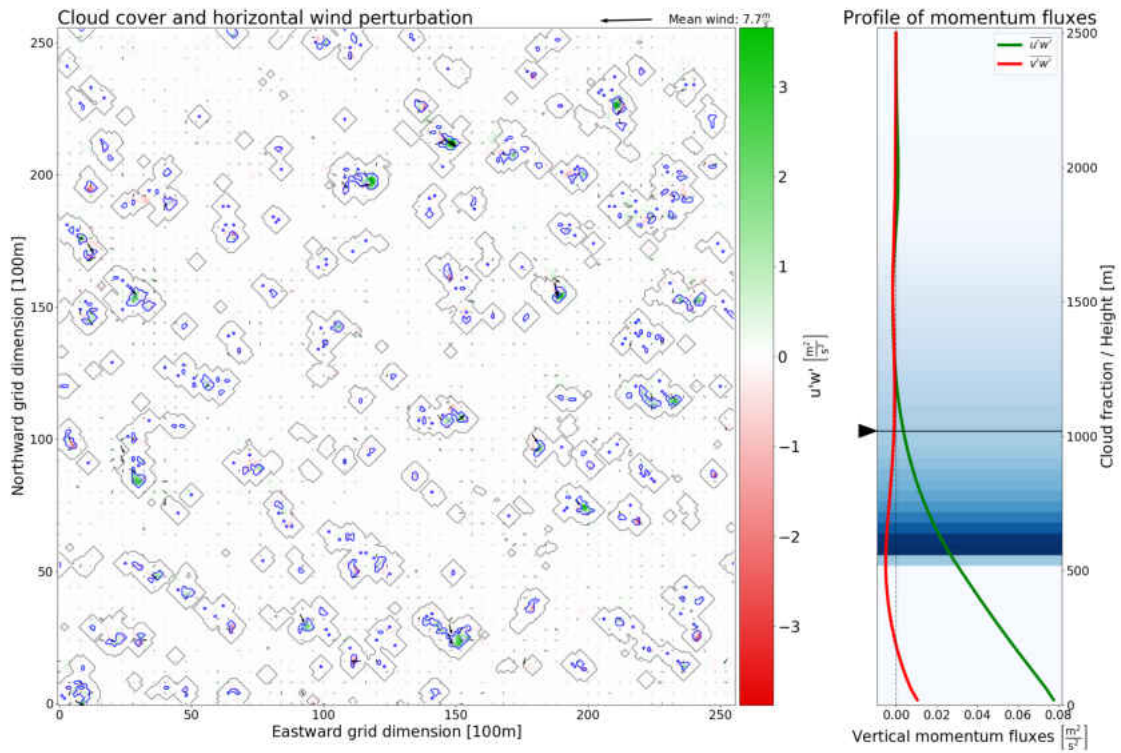horizontal wind perturbation+uw map, BOMEX, 256x256x63, dx=100m, dz=40.0m, t=360min, h=1020.0m

Figure 4.10: Horizontal slice for BOMEX case, h = 1020 m, $u'w'$ background. At this height we have a mix of cloud tops and mid sections, depending on the lifted air parcel. We observe, that the regions containing clouds have mostly positive flux. The cloud regions with negative flux are at cloud tops.

Chapter 5

Conclusion

5.1 Conclusion

To summarize our results, we have derived the second-moment momentum budgets for the Large-Eddy Simulation SAM. Simulations were performed on the UWM cluster with 256×256 horizontal grid points and a simulation time of six and four hours, for the BOMEX shallow cumulus and the DYCOMSII-RF01 stratocumulus cases, respectively. Comparing the budget plots to those shown by Heinze et al. (2015), we see a general agreement for the DYCOMS stratocumulus case. For the BOMEX shallow cumulus case however, we found and an agreement in trends, but a deviation near ground level, where the SAM budgets change direction. Additionally, there is a scaling factor of around 2 between the SAM and Heinze budget terms above cloud base.

Based on the large $\overline{u'^2}$ and $\overline{w'^2}$ profiles but a small $\overline{u'w'}$ in the cloud top region for the BOMEX, we investigated the horizontal momentum distribution. For this purpose, a plotting tool was developed, which shows the local wind strengths and directions, cloud cover, and momentum fluxes in horizontal slices of the three-dimensional model grid. These plots show a generally positive $\overline{u'w'}$ within clouds, while we have regions of negative momentum flux within the clouds' halo region and at cloud top. Conditional profile plots for $\overline{u'w'}$ support this finding, showing opposite signs of the in-cloud and environmental momentum flux. Above cloud top and in the environment between clouds, we find a significant contribution to the momentum flux, suggesting the presence of gravity waves, likely caused by the buoyant updrafts.

Due to the specific conditions of the BOMEX case, namely a jet maximum in the eastward mean wind profile paired with local regions of updraft, we have a zone of upgradient flux directly above the jet maximum between 800 and 1000 m, as seen in conditional profiles of the eastward mean wind. This zone coincides with the lower part of the region with small $\overline{u'w'}$. This is caused by the inertia of the rising air parcel, delaying its adjustment to the mean wind speed of the environment. This contradicts the general assumption, that all fluxes are directed downgradient, calling into question a number of methods of approximation for fluxes used in atmospheric simulations.

5.2 Outlook

There is some future work to improve the results presented in this thesis which will be listed here. It was noted in section 3.2 that the method of finding the cloud halo region is not based on model data, but geometric considerations. This introduces some error to the conditional plots including this region. Therefore, finding a method to define the halo more accurately will improve the results and might help describe differences of the three regions discussed.

Running SAM with the grid parameters used by Heinze et al. (2015) will reveal whether the differences observed in the budget plots are a result of the disparity in grid spacing and size. If the differences near ground level persist even when using the same grid, looking into the causes might provide new insights into momentum fluxes near ground level or at the very least improve atmospheric modeling near the grid boundary.

As was mentioned in subsection 4.2.1, the conditional profiles for the BOMEX case contain a lot of noise above $2100\,\mathrm{m}$ due to low cloud fraction at these heights. Sampling three-dimensional data over a time interval of an hour should reduce the noise and improve the profile plots.

Bibliography

at University of Wisconsin Milwaukee, H. P. C., 2019a: Hardware specifications | high performance computing.

at University of Wisconsin Milwaukee, H. P. C., 2019b: Software and operating system | high performance computing.

community, T. S., 2019: Overview — numpy v1.16 manual.

Foundation, P. S., 2016: Overview — python 2.7.13 documentation.

Heinze, R., D. Mironov, and S. Raasch, 2015: Second-moment budgets in cloud topped boundary layers: A large-eddy simulation study. *Journal of Advances in Modeling Earth Systems*, **7**, 510–536.

HOLLAND, J. Z. and E. M. RASMUSSON, 1973: Measurements of the atmospheric mass, energy, and momentum budgets over a 500-kilometer square of tropical ocean. *Monthly Weather Review*, **101**, 44–55.

Hunter, J., D. Dale, E. Firing, M. Droettboom, and the Matplotlib development team, 2018: Matplotlib: Python plotting — matplotlib 2.2.3 documentation.

Khairoutdinov, M. F. and D. A. Randall, 2003: Cloud resolving modeling of the arm summer 1997 iop: Model formulation, results, uncertainties, and sensitivities. *Journal of the Atmospheric Sciences*, **60**, 607–625.

Larson, V. E., 2017: *CLUBB-SILHS: A parameterization of subgrid variability in the atmosphere.*

Siebesma, A. P., C. S. Bretherton, A. Brown, A. Chlond, J. Cuxart, P. G. Duynkerke, H. Jiang, M. Khairoutdinov, D. Lewellen, C.-H. Moeng, E. Sanchez, B. Stevens, and D. E. Stevens, 2003: A large eddy simulation intercomparison study of shallow cumulus convection. *Journal of the Atmospheric Sciences*, **60**, 1201–1219.

Stevens, B., D. H. Lenschow, G. Vali, H. Gerber, A. Bandy, B. Blomquist, J. L. Brenguier, C. S. Bretherton, F. Burnet, T. Campos, S. Chai, I. Faloona, D. Friesen, S. Haimov, K. Laursen, D. K. Lilly, S. M. Loehrer, S. P. Malinowski, B. Morley, M. D. Petters, D. C. Rogers, L. Russell, V. Savic-Jovcic, J. R. Snider, D. Straub, M. J. Szumowski, H. Takagi, D. C. Thornton, M. Tschudi, C. Twohy, M. Wetzel, and M. C. van Zanten, 2003: Dynamics and chemistry of marine stratocumulus—dycoms-ii. *Bulletin of the American Meteorological Society*, **84**, 579–594.

Stevens, B., C.-H. Moeng, A. S. Ackerman, C. S. Bretherton, A. Chlond, S. de Roode, J. Edwards, J.-C. Golaz, H. Jiang, M. Khairoutdinov, M. P. Kirkpatrick, D. C. Lewellen, A. Lock, F. Müller, D. E. Stevens, E. Whelan, and P. Zhu, 2005: Evaluation of large-eddy simulations via observations of nocturnal marine stratocumulus. *Monthly Weather Review*, **133**, 1443–1462.

Stull, R., 2012: *An Introduction to Boundary Layer Meteorology*. Atmospheric and Oceanographic Sciences Library, Springer Netherlands.

Whitaker, J., 2017: netcdf4 api documentation.

Wikipedia contributors, 2019: Dilation (morphology) — Wikipedia, the free encyclopedia. https://en.wikipedia.org/w/index.php?title=Dilation_(morphology)&oldid=885533893. [Online; accessed 14-April-2019].